Journal of Power Sources 253 (2014) 205–213

Contents lists available at ScienceDirect

Journal of Power Sources

journal homepage: www.elsevier.com/locate/jpowsour

Superior capacitive performances of binary nickel–cobalt hydroxide nanonetwork prepared by cathodic deposition

Jia-Cing Chen, Chun-Tsung Hsu, Chi-Chang Hu*

Laboratory of Electrochemistry and Advanced Materials, Department of Chemical Engineering, National Tsing Hua University, Hsin-Chu 30013, Taiwan

HIGHLIGHTS

- $Ni_{0.32}Co_{0.68}(OH)_2$ shows C_S of 1000 F g^{-1}, 100% C_S cycle-retention, and 69% C_S rate-retention at 500 mV s^{-1}.
- $Ni_{0.32}Co_{0.68}(OH)_2$ is desired for the asymmetric design with 90% energy efficiency at 10 A g^{-1}.
- Small current densities facilitate the formation of porous nanonetwork microstructures.
- pH and deposition temperature affect the Co/Ni ratio and capacitive performances of $Ni_xCo_{1-x}(OH)_2$.

GRAPHICAL ABSTRACT

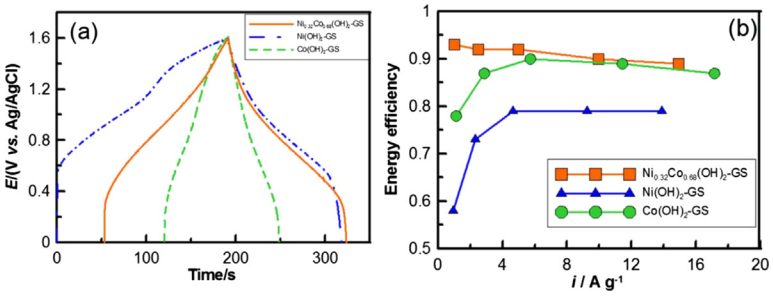

ARTICLE INFO

Article history:
Received 4 October 2013
Received in revised form
25 November 2013
Accepted 16 December 2013
Available online 21 December 2013

Keywords:
Nickel–cobalt hydroxide
Cathodic deposition
Porous nanonetwork
Superior capacitive performances
Asymmetric supercapacitor

ABSTRACT

Binary nickel–cobalt hydroxides (denoted as $Ni_xCo_{1-x}(OH)_2$) with advanced capacitive performances, such as the superior rate capability, energy efficiency, and capacitance rate-/cycle-retention, are synthesized by cathodic deposition. The effects of deposition variables are systematically investigated and discussed. The deposition current density has been found to determine the morphology of hydroxides whereby a small current density facilitates the formation of porous nanonetwork microstructures. Both pH and temperature of the precursor solution affect the Co/Ni ratio of hydroxides, which in turn influence the capacitive performances. Eventually, $Ni_{0.32}Co_{0.68}(OH)_2$ synthesized under our proposed deposition condition exhibits a specific capacitance value of ca. 1000 F g^{-1} at 5 mV s^{-1}, 100% capacitance cycle-retention over 1000 cycles, and 69% capacitance rate-retention (varying from 5 to 500 mV s^{-1}). These superior capacitive performances make $Ni_{0.32}Co_{0.68}(OH)_2$ a promising material of the positive electrode for an asymmetric supercapacitor with an energy efficiency of 90% at 10 A g^{-1}.

1. Introduction

Energy storage has been a critical concern as the demands of energy supply become challenging in recent years. For instance, high-tech products such as mobile phones and hybrid electric vehicles/electric vehicles require the power supply system with both high energy density and high power supply at the same time. However, even though newly-developed batteries, like lithium batteries [1] and fuel cells [2], retain very high specific energy, the high power supply is still an issue. Accordingly, electrochemical capacitors (ECs), also known as supercapacitors, have attracted plenty of attention because they show the promising potential to meet such energy-storing demands, not to mention their extremely long cycle life [3].

ECs can be sorted into two types by the mechanism of energy storage. The electrical double-layer capacitors (EDLCs) store energy

* Corresponding author. Department of Chemical Engineering, National Tsing Hua University, 101, Section 2, Kuang-Fu Road, Hsin-Chu 30013, Taiwan. Tel./fax: +886 3 5736027.
E-mail address: cchu@che.nthu.edu.tw (C.-C. Hu).
URL: http://mx.nthu.edu.tw/~cchu/

0378-7753/$ – see front matter © 2013 Elsevier B.V. All rights reserved.
http://dx.doi.org/10.1016/j.jpowsour.2013.12.073

by the electrical double-layer formed at the interface between electrode and electrolyte with their specific capacitance mainly determined by the electrolyte-accessible surface area [3]. The pseudocapacitors, on the other hand, utilizing surface redox reactions of electrochemically active materials generally show higher specific capacitance than porous carbons [3,4]. Furthermore, designed porous microstructures of such active materials have been proposed to simultaneously enhance the utilization of double-layer and redox capacitances [5], leading to extensive research attention in the materials sciences/engineering. Recently, in order to enhance the specific energy of devices, asymmetric supercapacitors consisting of two different electrode materials with complementary working potential windows are designed to broaden their cell voltage [6].

Undoubtedly, specific energy is an important property in developing ECs [6], but seems to be overemphasized in the research field. The cell voltage plays a crucial role in specific energy of ECs [6], while ECs with high specific energy but poor energy efficiency could generate huge heat during discharge because of the significant energy loss [7]. Also, drastic temperature increase might happen at high discharge rates, which not only damages the capacitive performances but also leaves the whole cell under a dangerous state. The energy efficiency of a device generally depends on the electrochemical reversibility of electroactive materials on both electrodes [3], although the influence of *iR* drop on the energy efficiency becomes more significant at higher rates. Accordingly, the original asymmetric supercapacitor consisting of a battery-type material and one double-layer-type material [8] has to be redesigned since the enhanced specific energy of such systems generally comes with the trade-off in specific power [6] because of the worse electrochemical reversibility of the battery-type materials in one of the electrodes. Moreover, the charge capacity of the battery-type electrode must be much larger than that of the double-layer one because 80% (or more) loss in the charge capacity at very high rates is commonly found for a battery-type material [7,9]. This effect also reduces the specific energy (i.e., specific energy is not optimized). Therefore, how to improve the electrochemical reversibility of a battery-type material (e.g., $Ni(OH)_2$ in this work) with a complementary working potential window to its double-layer-type counterpart is the new challenge in developing ECs of the asymmetric design.

For pseudocapacitive materials, RuO_2 is well known to be an ideal compound with superior reversibility and high specific capacitance [3,10]. However, due to its high cost and environmental issues, RuO_2 cannot be widely commercialized. Therefore, many researchers paid much attention on utilizing nickel and cobalt oxides/hydroxides because of being cost-effective and environmentally friendly [7,11]. Recently, binary Ni–Co oxides/hydroxides have been of interests because of their enhanced characteristics over the individual materials [12]. The doping of Co^{2+} into the nickel oxide was found to improve the utilization of electroactive materials, depress the capacity loss during long charge–discharge cycles, decrease the redox peak potential difference (ΔE_P), and increase the electronic conductivity [13–19]. As a result, many studies focused on synthesis and characterization of $Ni_xCo_{1-x}(OH)_2$ and $NiCo_2O_4$ for the asymmetric supercapacitors. For example, Co_xNi_{1-x} layered double hydroxides (LDHs) by both chemical co-precipitation and potentiostatic deposition showed specific capacitance of 1809 and 2104 F g^{-1}, respectively [20,21]. Meanwhile, mesoporous Co_3O_4/$Ni(OH)_2$ nanosheet networks were reported to exhibit specific capacitance of 1144 F g^{-1} [22]. Nonetheless, several challenges, such as energy efficiency and joule-heating effect at high discharge rates as well as the long-term cycle life, need to be addressed for utilizing binary Ni–Co oxy-hydroxides.

In this work, $Ni_xCo_{1-x}(OH)_2$ was prepared by electrochemical deposition because of many advantages: (1) one-step process and low-cost equipment, (2) low operation temperature and energy-saving, (3) direct deposition onto porous/curved surfaces without binders, and (4) easy control on thickness, composition, and microstructure by varying deposition parameters, although several methods have been proposed to enhance the performances, such as chemical precipitation, sol–gel [23–25], sputtering [26], thermal decomposition [27,28] and electrochemical deposition [29–31]. Moreover, cathodic deposition was employed to synthesize $Ni_xCo_{1-x}(OH)_2$ in the attempt to synergistically attain the high specific capacitance from $Ni(OH)_2$ (battery material) and the high reversibility from $Co(OH)_2$ (capacitor material). This method was applied because the capacitive characteristics of deposits could be effectively controlled by varying the deposition variables. The effects of deposition factors on the capacitive performances were systematically discussed to give a fundamental understanding in order to approach superior capacitive performances. Eventually, $Ni_{0.32}Co_{0.68}(OH)_2$ synthesized under our proposed deposition condition exhibits excellent performances in energy efficiency and cycle life retention, credited to the synergistic effect of $Ni(OH)_2$ and $Co(OH)_2$.

2. Experimental

$Ni_xCo_{1-x}(OH)_2$ was cathodically deposited onto 10 × 10 × 3 mm graphite substrates from the deposition baths containing 60 mM $NaNO_3$, $NiCl_2{\cdot}6H_2O$, and $CoCl_2{\cdot}6H_2O$ in variable concentrations. The substrate preparation and pre-treatment procedures followed our previous work [32]. The substrates were carefully coated with a thick film of PTFE with an exposed surface area of 1 cm^2. The deposition variables studied in this work include the Ni/Co ratio, temperature, pH of the deposition bath, and the deposition current density. Typically, $Ni_xCo_{1-x}(OH)_2$ was deposited at 1 mA cm^{-2} for 750 s (see Fig. S1 and Table S1) from a bath with the Co^{2+}/Ni^{2+} ratio = 2 at 70 °C [7,22,29,33]. The passed charge density of deposition is constant (0.75 C cm^{-2}) meanwhile the total concentration of Co^{2+} and Ni^{2+} was fixed at 30 mM. After deposition, the PTFE film was removed and the deposits were rinsed with deionized water several times and dried at room temperature under a reduced pressure. The mass of all hydroxide deposits was measured by an analytical balance (XS105DU, Mettler Toledo, Switzerland) with its minimum digit at 0.01 mg. The mass of all deposits has been confirmed to be 0.5 ± 0.05 mg cm^{-2} with the exception of the deposit prepared at 14 mA cm^{-2}.

The electrochemical characteristics of $Ni_xCo_{1-x}(OH)_2$ were examined by an electrochemical analyzer (CHI633c, CH Instruments) in 1 M NaOH. The reference and counter electrodes in the three-electrode system were Ag/AgCl (Argenthal, 3 M KCl, 0.207 V vs. SHE at 25 °C) and a platinum wire (99.95%, 0.5 mm in diameter and 8 cm in length), respectively. A Luggin capillary was used to minimize errors due to *iR* drop in the electrolytes. The specific capacitance value of all binary hydroxide deposits was estimated from CV curves using the following equation:

$$C_S = \frac{1}{m(V_{SU} - V_{SL})} \int_{V_{SL}}^{V_{SU}} I\mathrm{d}t = \frac{1}{m(V_{SU} - V_{SL})} \int_{V_{SL}}^{V_{SU}} I\left(\frac{\mathrm{d}V}{v}\right)$$

where C_S is the specific capacitance (F g^{-1}); m is the mass of the pseudocapacitive material (g); v is the potential scan rate (V s^{-1}); V_{SU} and V_{SL} are the integration limits of the voltammetric curve (in V); and I denotes the response current (A). Note that in order to avoid any possible contribution from the oxygen evolution reaction,

only the cathodic currents on the negative sweeps were employed for the integration.

The surface morphology of hydroxide deposits was examined by a field-emission scanning electron microscope (Hitachi S-4700I). The composition of $Ni_xCo_{1-x}(OH)_2$ was examined by energy dispersive spectrometer (EDS) and some samples have been confirmed by means of the inductively coupled plasma (ICP) analysis. X-ray diffraction (XRD) patterns were obtained from an X-ray powder diffractometer (Cu Kα, Ultima IV, Rigaku).

For the full cell test of the asymmetric supercapacitor, $Ni_{0.32}Co_{0.68}(OH)_2$ and reduced graphene oxide (RGO) worked as the positive and negative electrodes, respectively. The GO solutions were prepared according to the modified Hummers' method with supersonic exfoliation [34] with nano-graphite platelets (N008-100-N, Angstron Materials Co., USA) being employed as the raw material. RGO was obtained via the microwave-assisted hydrothermal procedure by a microwave reactor (CEM, USA) heating to 170 °C and holding at this temperature for 5 min [35]. The charge–discharge curves of asymmetric ECs were measured at different current densities to evaluate the specific energy, specific power, and energy efficiency. All solutions were prepared with deionized water produced by a reagent water system (Milli-Q SP, Japan) at 18 MΩ cm. The solution temperature was maintained at specified temperatures with an accuracy of 0.1 °C by a water thermostat (Haake DC3 and K20). The electrolyte, 1 M NaOH, was degassed with purified N_2 for 30 min before electrochemical measurements. This nitrogen was passed over the electrolyte during the measurements.

3. Results and discussion

3.1. Effects of deposition current density

Fig. 1a shows the typical linear sweep voltammogram (LSV) of graphite measured in the deposition bath containing 20 mM $CoCl_2{\cdot}6H_2O$, 10 mM $NiCl_2{\cdot}6H_2O$, and 60 mM $NaNO_3$. As the potential was negatively scanned from 0.4 V, the small reduction current density (ca. 0.5 mA cm^{-2}) from −0.4 to −0.63 V indicates the slow reduction rate of NO_3^- in this potential region. The reduction of NO_3^- at the surface of graphite generates OH^- to deposit $Ni_xCo_{1-x}(OH)_2$ because of the localized, concentrated OH^-. When the potentials were more negative than −0.63 V, the current density of NO_3^- reduction significantly increased and two waves were visible at ca. −0.78 and −1.25 V, probably due to the complicated mechanism of NO_3^- reduction [36] and/or the catalytic effect of hydroxides [7]. During the LSV test, a thick and dense green deposit could be observed as the potentials were negative to −0.9 V. As the potentials were scanned to −1.3 V, a light-green deposit was formed, indicating the extensive deposition of hydroxides. Bubbles evolved beyond −1.4 V, attributable to hydrogen evolution [37]. Since hydroxides precipitated at different potentials might show distinct properties, four current densities, i.e., 0.5, 1, 5, and 14 mA cm^{-2}, were chosen to deposit binary $Ni_xCo_{1-x}(OH)_2$.

All CV curves of $Ni_xCo_{1-x}(OH)_2$ deposited at different current densities (Fig. 1b) show an anodic shoulder around 0.1 V, which was positively shifted with increasing the deposition current density. The presence of this shoulder between 0.05 and 0.1 V on the positive sweep is attributable to the Co(II) → Co(III) transition on the basis of the similar peak potential [7]. The deposits prepared at higher current densities exhibited smaller redox current density. The above results suggest the atomic scale mixing of $Ni(OH)_2$ and $Co(OH)_2$ since the voltammetric responses of these hydroxides are very different from those of $Ni(OH)_2$ and $Co(OH)_2$. The specific capacitance estimated from the negative scan of CVs is equal to 930, 949, 834, and 512 F g^{-1} for the $Ni_xCo_{1-x}(OH)_2$ deposited at 0.5, 1, 5, and 14 mA cm^{-2}, respectively. The specific capacitance and CV

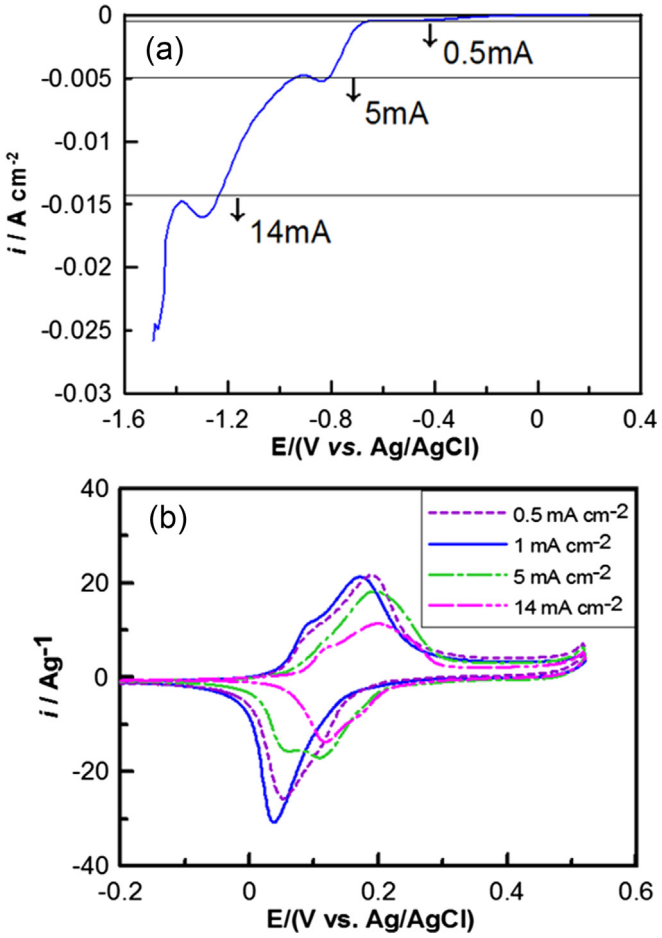

Fig. 1. (a) A linear sweep voltammogram measured at 2 mV s^{-1} from a bath containing 60 mM $NaNO_3$, 20 mM $CoCl_2{\cdot}6H_2O$, and 10 mM $NiCl_2{\cdot}6H_2O$ at 70 °C. (b) Cyclic voltammograms measured at 5 mV s^{-1} in 1 M NaOH for $Ni_xCo_{1-x}(OH)_2$ deposited from the above solution at 0.5, 1, 5, 14 mA cm^{-2}.

behaviour of $Ni_xCo_{1-x}(OH)_2$ deposited at 0.5 and 1 mA cm^{-2} were roughly same, indicating the formation of an identical compound. Thus, 1 mA cm^{-2} is the preferred current density of deposition because of time-saving. On the other hand, the distinctive *i–E* behaviour for the deposits prepared at 1, 5, and 14 mA cm^{-2} may result from the microstructure difference (e.g., morphology, composition, crystallinity, etc.). For example, the positive shift in the redox peaks and decrease in the C_S of $Ni_xCo_{1-x}(OH)_2$ is probably due to the change in the Ni/Co ratio within the deposits caused by varying the deposition current density.

SEM images in Fig. 2 were taken to examine the morphology of $Ni_xCo_{1-x}(OH)_2$ since the morphology was reported to influence the rates of ion transport and electron conduction [22]. Clearly, the morphologies of deposits prepared at 0.5 and 1 mA cm^{-2} (Fig. 2a and b) are almost the same, which composed of inter-connected platelets and irregular pores. The same morphology correlated well to their similar capacitive behaviour. On the other hand, the platelet structure could only be found implicitly for the $Ni_xCo_{1-x}(OH)_2$ deposit prepared at 5 mA cm^{-2} (Fig. 2c), while the whole surface with very few pores was covered with broad sheets. Such morphology hinders electrolytes from penetrating into active materials, so less active sites can be reached, resulting in a decrease of the specific capacitance. Fig. 2d reveals that broad sheets are still dominant but become fragmented for the deposit synthesized at 14 mA cm^{-2}.

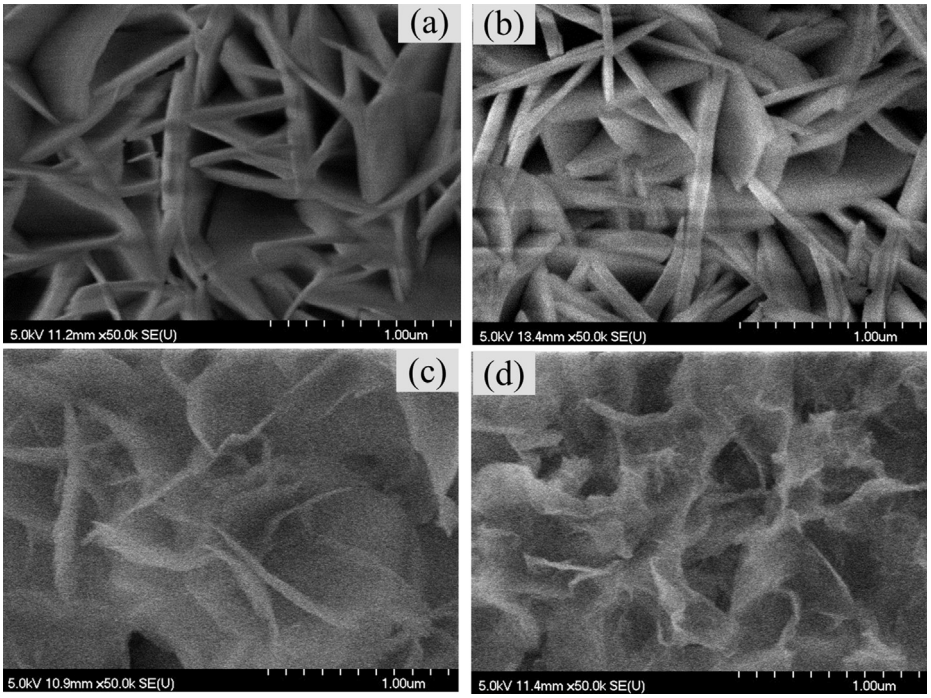

Fig. 2. SEM images of $Ni_xCo_{1-x}(OH)_2$ deposits prepared at (a) 0.5, (b) 1, (c) 5, (d) 14 mA cm^{-2} from a bath containing 60 mM $NaNO_3$, 20 mM $CoCl_2 \cdot 6H_2O$, and 10 mM $NiCl_2 \cdot 6H_2O$ at 70 °C.

All the differences in morphologies caused by varying the deposition current density may be attributed to the deposition rate. Note that the platelet structure in Fig. 2a and b can be considered vertically-standing sheets, representing a preferred orientation at a slow deposition rate. As the deposition current increases, the deposition rate also accelerates due to a higher OH^- concentration resulting from a higher rate of NO_3^- reduction. As a result, hydroxides are forced to directly deposit on the electrode surface and once the deposition rate is too high to effectively rearrange the newly deposited species (similar to ad-atoms), the platelet structure cannot be formed, leading to the broad sheet structure. In addition, the fragmented sheets at 14 mA cm^{-2} were likely due to the minor hydrogen evolution reaction.

The morphologies seem to result from the nucleation type, i.e., the instantaneous nucleation or the progressive nucleation. Fig. 3 shows the schematic representation of the nucleation models at low and high deposition current densities. At a high current density

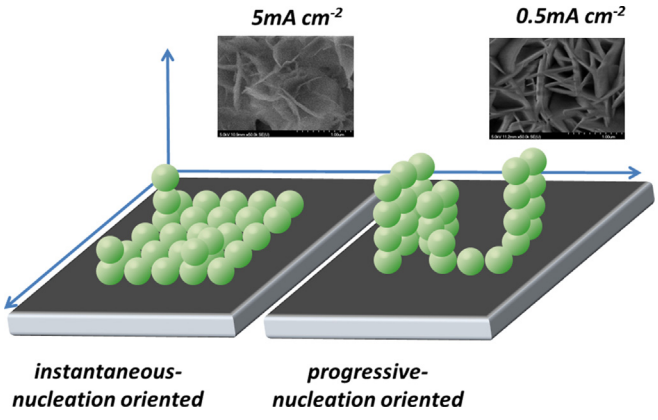

Fig. 3. The schematic representation of the nucleation models at different deposition current densities.

(e.g., ≥5 mA cm^{-2}), an instantaneous nucleation mode is favourable. In this model, the rate of nucleation is very rapid in comparing with the rate of crystal growth [38]. Nuclei are formed within a very short time and the coverage rate of electrode surface sites by hydroxide deposition should be very fast. Two-dimensional growth like horizontal sheets is hence preferable. On the other hand, at a low current density like 0.5 mA cm^{-1}, a progressive nucleation process is preferred. Under this model, the rate of crystal growth is higher than that of nucleation, and nuclei are continuously formed as the crystals grow. Therefore, thick and vertically-standing sheets are obtained. Though there is no direct evidence correlating the nucleation type and morphology in this work, a similar finding has been reported by Noam Eliaz and Moshe Eliyahu [38]. They found that electrodeposition of hydroxyapatites involved both instantaneous nucleation (two-dimensional growth) and progressive nucleation (three dimensional growth). Since the cathodic deposition of hydroxides in present study also involves an electrochemical reduction step (i.e., NO_3^- reduction) followed by a chemical precipitation step (i.e., $Ni_xCo_{1-x}(OH)_2$ formation), the influence of the chemical precipitation kinetics on the microstructures of deposits is plausible. Finally, the redox reaction of $Ni_xCo_{1-x}(OH)_2$ involves ion exchange in the electrolytes [32,39], so the facility of ion transfer becomes very critical. The interconnected platelets are therefore favourable. Hence, 1 mA cm^{-2} is chosen to deposit $Ni_xCo_{1-x}(OH)_2$ with the largest specific capacitance.

3.2. Effects of pH in the deposition bath

The effects of pH in the deposition bath on the microstructures and capacitive performances of $Ni_xCo_{1-x}(OH)_2$ are shown in Table 1. The specific capacitance of $Ni_xCo_{1-x}(OH)_2$ synthesized in the pH range of investigation is generally similar. However, as the pH value was elevated to 7, a few green particles have been found to be suspended in the deposition bath. When the pH value was 7.8, many green particles were visible in the deposition bath which

Table 1
The specific capacitance (C_S) measured at 5 mV s^{-1}, the capacitance rate-retention with the scan rate of CV varying from 5 to 500 mV s^{-1}, and the Co/Ni ratio of the as-deposited $Ni_xCo_{1-x}(OH)_2$ prepared from the deposition baths with different pH values. The Co/Ni ratios were deduced from the EDS results.

pH	4	5	6	7	7.8
C_s (F g^{-1})	875	879	877	822	908
Rate retention (%)	69	67	70	68	63
Co/Ni ratio	0.96	1.65	2	2.44	0.69

should be not suitable for hydroxide deposition. The precipitation of green hydroxides without NO_3^- reduction is reasonable since hydroxide precipitation has been reported to occur at pH around/above 7 [40]. Accordingly, the variation in the specific capacitance and capacitance retention at pH $\geq$ 7 is possibly attributed to the minor variation in the $Ni_xCo_{1-x}(OH)_2$ composition, especially for the small drop of the capacitance retention at pH = 7.8.

Based on the above discussion, the composition of the deposition bath might be changed due to the pre-precipitation of hydroxides. Therefore, EDS analysis is performed to check the composition of resultant $Ni_xCo_{1-x}(OH)_2$. From Table 1, the Co/Ni ratio increases with pH of the deposition bath from 4 to 7. This result is attributed to the higher rate of $Co(OH)_2$ formation at a higher pH value in comparison with $Ni(OH)_2$ formation, which is reasonably explained by its smaller solubility equilibrium constant (K_{sp}) of $Co(OH)_2$ [41]. However, an obvious drop in the Co/Ni ratio is found at pH = 7.8 in comparison with other pH values, probably due to its lower Co^{2+} concentration in the deposition bath because of the more precipitation of $Co(OH)_2$ at this pH value. It is noticeable that the Co/Ni ratio is same as that in the deposition bath when pH of the deposition bath is 6. Based on the above results and discussion, pH of 6 is chosen to be the preferred condition to attain both high capacitance and high rate retention.

3.3. Effects of the deposition bath temperature

Fig. 4a shows the chronopotentiograms (CPs) obtained at 1 mA cm^{-2} from a solution containing 60 mM $NaNO_3$, 20 mM $CoCl_2 \cdot 6H_2O$, and 10 mM $NiCl_2 \cdot 6H_2O$ with temperatures varying from 25 to 70 °C. All the curves in Fig. 4a exhibit a similar shape while the steady-state potential of deposition is monotonously shifted to a less negative value at a higher deposition temperature. This result indicates easier electrochemical reduction of NO_3^- at a higher temperature. The sharply negative movement of the electrode potential to a certain value at the beginning of deposition is attributable to the double-layer charging effect. Afterwards, a small peak is found, possibly due to a nucleation process of hydroxides. Thereafter, the deposition potential becomes rather stable (i.e., the steady-state potential).

Fig. 4b–d shows the surface morphology of various deposits fabricated at 25, 40, and 70 °C, respectively. Obviously, the deposition temperature affects the morphology of deposits. In Fig. 4b (70 °C), thick platelets are interconnected and macropores are obvious. From Fig. 4c (40 °C), the platelet structure becomes thin and broad sheets are formed so that pores could barely be spotted. In Fig. 4d (25 °C), the morphology is similar to that obtained at 40 °C (see Fig. 4c), but the size of both platelets and sheets shrinks. In comparison with Fig. 4b (70 °C), the deposit obtained at 25 °C seems to have more nucleation sites of platelets, but fails to grow thick. Such a morphology difference is substantial and will show significant influences on the capacitive performance.

Table 2 shows the specific capacitance and capacitance rate-retention of hydroxides deposited at the temperature varying from 25 to 70 °C. The specific capacitance of the deposits prepared at 40–70 °C shows roughly the same level around 980 ± 40 F g^{-1}, while C_S for the deposit fabricated at 25 °C drastically drops to 871 F g^{-1}. Moreover, as the deposition temperature decreases, the capacitance rate-retention gradually increases. Both effects suggest

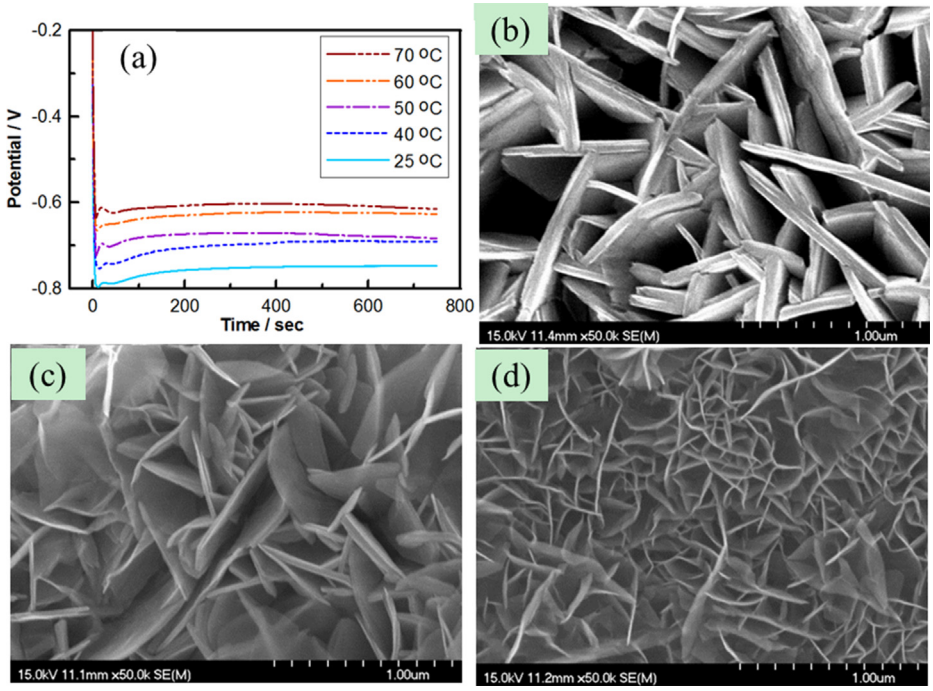

Fig. 4. (a) Chronopotentiograms obtained at 1 mA cm^{-2} from a solution containing 60 mM $NaNO_3$, 20 mM $CoCl_2 \cdot 6H_2O$, and 10 mM $NiCl_2 \cdot 6H_2O$ at 25–70 °C. The equilibrium potential of the Ag/AgCl reference electrode has been compensated at the corresponding temperature. (b, c, d) SEM images of $Ni_xCo_{1-x}(OH)_2$ deposited at (b) 70, (c) 40, and (d) 25 °C.

Table 2
The specific capacitance (C_S) measured at 5 mV s^{-1} and the capacitance rate-retention from 5 to 500 mV s^{-1} of $Ni_xCo_{1-x}(OH)_2$ prepared from a deposition bath containing 60 mM $NaNO_3$, 20 mM $CoCl_2 \cdot 6H_2O$, and 10 mM $NiCl_2 \cdot 6H_2O$ at 25–70 °C.

	25 °C	40 °C	50 °C	60 °C	70 °C
C_s (F g^{-1})	871	962	1035	940	989
Rate retention (%)	76%	66%	64%	61%	61%

the possible variation in the composition of hydroxides by changing the deposition temperature because the hydroxides deposited at lower temperatures exhibit the more $Co(OH)_2$-like capacitive performances. The above speculation is supported by the EDS analysis for the hydroxides deposited at 25, 50 and 70 °C (see Table 3). Clearly, the Co/Ni ratio of $Ni_xCo_{1-x}(OH)_2$ deposited at 70 °C is approximately same as that of the deposition bath, so the composition control of $Ni_xCo_{1-x}(OH)_2$ is easy by varying the bath composition for this deposition temperature. Accordingly, 70 °C is set as the preferred deposition temperature for preparing $Ni_xCo_{1-x}(OH)_2$. When the temperature becomes lower, the content of cobalt within the hydroxides is drastically increased. Due to the fact that the Co/Ni ratio of $Ni_xCo_{1-x}(OH)_2$ deposited at 70 °C is twice of that at 25 °C, the deposition rate of cobalt hydroxide is much faster than that of nickel hydroxide at a low temperature (see Fig. S2). This phenomenon suggests a higher activation energy of $Ni(OH)_2$ precipitation in comparing with $Co(OH)_2$ precipitation. Therefore, the slow deposition kinetics of $Ni(OH)_2$ can be accelerated at higher temperatures since the temperature effect on enhancing the hydroxide deposition rate is more obvious for $Ni(OH)_2$. Since the surface morphologies of $Ni(OH)_2$ and $Co(OH)_2$ are intrinsically different [42,43], the variation in the morphology of $Ni_xCo_{1-x}(OH)_2$ shown in Fig. 4b–d might result from the composition effect.

After the above examinations of deposition current density, deposition time, pH of the deposition bath, and deposition temperature, $Ni_xCo_{1-x}(OH)_2$ deposits with excellent capacitive performances are proposed to be prepared at a cathodic current density of 1 mA cm^{-2} for 750 s from the deposition bath at pH of 6 under 70 °C. Under the proposed deposition conditions, the composition of deposits can be easily and precisely controlled in order to attain results with good reproducibility. Furthermore, these hydroxide deposits with their composition approximately identical to that in the deposition bath generally show comparatively high specific capacitance and good capacitance rate-retention. Accordingly, the effect of bath composition can be investigated.

3.4. Effects of the Co^{2+}/Ni^{2+} ratio in the deposition bath

Fig. 5 shows the CV curves of $Ni_xCo_{1-x}(OH)_2$ deposited from the baths with the Co^{2+}/Ni^{2+} ratio varying from 0.5 to 2. Obviously, as the Co^{2+}/Ni^{2+} ratio ascends, the anodic and cathodic peak potentials coincidentally shift to the less positive values. This phenomenon is reasonably due to the increase of the Co content in the hydroxides because the redox potential range of $Co(OH)_2$ (between 0 and 0.1 V) is less positive than that of $Ni(OH)_2$ (between 0.25 and 0.4 V). Moreover, the anodic peak becomes broader with increasing

Table 3
The Ni, Co, and O contents in $Ni_xCo_{1-x}(OH)_2$ prepared from a deposition bath containing 60 mM $NaNO_3$, 20 mM $CoCl_2 \cdot 6H_2O$, and 10 mM $NiCl_2 \cdot 6H_2O$ at 25, 50, and 70 °C.

	Ni (atomic %)	Co (atomic %)	O (atomic %)
70 °C	11	23	66
50 °C	9	26	65
25 °C	6	28	66

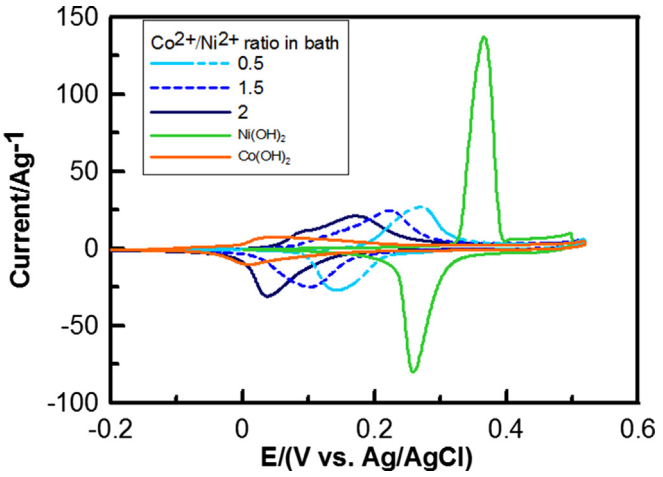

Fig. 5. CV curves measured at 5 mV s^{-1} in 1 M NaOH for $Ni_xCo_{1-x}(OH)_2$ deposited from the baths with the Co^{2+}/Ni^{2+} ratio varying from 0.5 to 2, as well as the individual $Ni(OH)_2$ and $Co(OH)_2$ deposited under similar conditions.

the cobalt content; meanwhile a shoulder is found at the Co^{2+}/Ni^{2+} ratio = 2. This shoulder wave, attributable to the Co(II) → Co(III) transition [7], significantly enhances the specific capacitance of $Ni_xCo_{1-x}(OH)_2$ since the specific capacitance estimated from the negative sweeps of CVs in Fig. 5 is 949, 935, 853, 810, and 784 F g^{-1} for deposits plated from the bath with the Co^{2+}/Ni^{2+} ratio = 2, 1.5, 1, 0.66, and 0.5, respectively.

Note the highest specific capacitance of $Ni_xCo_{1-x}(OH)_2$ deposited from the bath with the Co^{2+}/Ni^{2+} ratio = 2. This result is attributable to its broad anodic peak due to the dominant amount of Co within this hydroxide. Even though $Ni(OH)_2$, a typical battery material, exhibits an ultrahigh specific capacitance (e.g., 1350 F g^{-1} at 25 mV s^{-1} from Fig. 7), the increase in the Ni content does not guarantee higher specific capacitance of $Ni_xCo_{1-x}(OH)_2$ deposits. This result further supports the proposal that the metallic ions in the hydroxides matrix are under the atomic-scale mixing, which is not a simple mixture of $Ni(OH)_2$ and $Co(OH)_2$. This statement is strongly supported by the coincidentally negative shift in the anodic and cathodic peaks for the hydroxides with a higher Co content and the very different CV behaviour of a physical mixture of $Ni(OH)_2$ and $Co(OH)_2$ (see Fig. S3). Finally, a Co^{2+}/Ni^{2+} ratio of 2 in the deposition bath is chosen to be one of the preferred deposition conditions because of high specific capacitance. According to the EDS analysis (see Table S2 and Fig. S4), the deposit prepared at 1 mA cm^{-2} for 750 s from the bath containing 60 mM $NaNO_3$, 20 mM $CoCl_2 \cdot 6H_2O$, and 10 mM $NiCl_2 \cdot 6H_2O$ with pH of 6 at 70 °C is denoted as $Ni_{0.32}Co_{0.68}(OH)_2$.

3.5. Characterization and capacitive performances of $Ni_{0.32}Co_{0.68}(OH)_2$

Fig. 6 shows the typical XRD patterns of $Ni_{0.32}Co_{0.68}(OH)_2$, $Ni(OH)_2$, and $Co(OH)_2$ prepared by cathodic deposition under the identical conditions. The XRD pattern of $Ni_{0.32}Co_{0.68}(OH)_2$ is indexed partly from those of $Ni(OH)_2$ and $Co(OH)_2$, instead of all the characteristic peaks showing up. Peaks around 35° and 60° (in 2θ), probably from $Ni(OH)_2$, split into two peaks and show better crystalline quality in comparing with $Ni(OH)_2$. Again, the XRD patterns reveal that the $Ni_xCo_{1-x}(OH)_2$ deposits are not composed of a merely physical mixture of $Ni(OH)_2$ and $Co(OH)_2$. Since $Ni(OH)_2$ and $Co(OH)_2$ exhibit a similar crystalline structure and the size of Ni^{2+} and Co^{2+} is almost same, Ni^{2+} and Co^{2+} could replace each other in the crystalline sites of $Ni_xCo_{1-x}(OH)_2$. This phenomenon

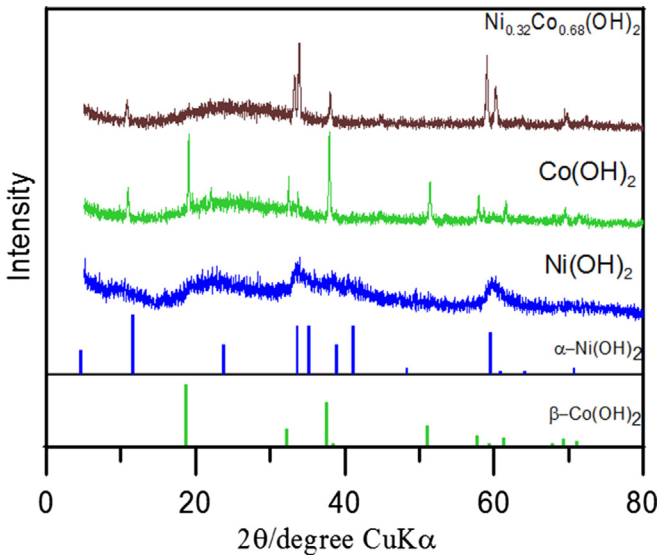

Fig. 6. XRD patterns of $Ni_{0.32}Co_{0.68}(OH)_2$, $Ni(OH)_2$ and $Co(OH)_2$ prepared by cathodic deposition under the identical preparation conditions.

induces the formation of atomically mixed $Co_xNi_{1-x}(OH)_2$ (probably layered double hydroxides, LDHs or solid solutions). As a result, it is hard to differentiate the exact phase of the binary hydroxides [21,44,45].

The atomically mixed $Co_xNi_{1-x}(OH)_2$ not only enhance the crystalline quality but also improve the capacitive performances. The redox behaviour of $Ni_{0.32}Co_{0.68}(OH)_2$ already illustrated the synergistic characteristics with a less positive redox potential window (similar to $Co(OH)_2$) and a high voltammetric charge (resembling $Ni(OH)_2$). The specific capacitance of $Ni(OH)_2$, $Ni_{0.32}Co_{0.68}(OH)_2$, and $Co(OH)_2$ measured at 5 mV s^{-1} is equal to 1731, 989, 678 F g^{-1}, respectively. The capacitance rate-retention of the above three deposits is equal to 7, 69, and 58%, respectively, when the scan rate of CV is increased from 5 to 500 mV s^{-1}. Interestingly, $Ni_{0.32}Co_{0.68}(OH)_2$ owns the best capacitance rate-retention and retains more than 60% of the specific capacitance of $Ni(OH)_2$. Again, due to the synergistic performances resulting from the atomically mixed Ni–Co hydroxides, $Ni_{0.32}Co_{0.68}(OH)_2$ is an excellent candidate for the positive electrode materials of aqueous asymmetric supercapacitors.

Fig. 7 shows the results of $Ni_{0.32}Co_{0.68}(OH)_2$, $Ni(OH)_2$, and $Co(OH)_2$ in a preliminary stability examination (i.e., a 1000-cycle stability test). Clearly, $Ni_{0.32}Co_{0.68}(OH)_2$ exhibits the superior capacitance stability and its specific capacitance remains almost constant. Note that the specific capacitance slightly increases and reaches a maximum (873 F g^{-1} at 25 mV s^{-1}) at about the 400th cycle. Afterwards, it keeps approximately constant in the following 600 cycles. On the contrary, the specific capacitance of $Ni(OH)_2$ monotonously decreases with its capacitance cycle-retention of 44%. The capacitance cycle-retention of $Co(OH)_2$ is 66%, which is also worse than $Ni_{0.32}Co_{0.68}(OH)_2$. Again, such an excellent synergistic effect on the cycle stability of $Ni_{0.32}Co_{0.68}(OH)_2$ is believed to result from the atomic mixing of Ni and Co hydroxides. This atomically mixed Ni–Co hydroxides might arrest the phase transformation and/or microstructure destruction since the phase conversion of $Ni(OH)_2$ and $Co(OH)_2$ has been reported to be a topotactic process [45]. All in all, $Ni_{0.32}Co_{0.68}(OH)_2$ shows the best cycle stability, the highest capacitance rate-retention (from 5 to 500 mV s^{-1}), and high specific capacitance close to 1000 F g^{-1}. Such superior capacitive performances can be credited to the synergistic effects of $Ni(OH)_2$ and $Co(OH)_2$.

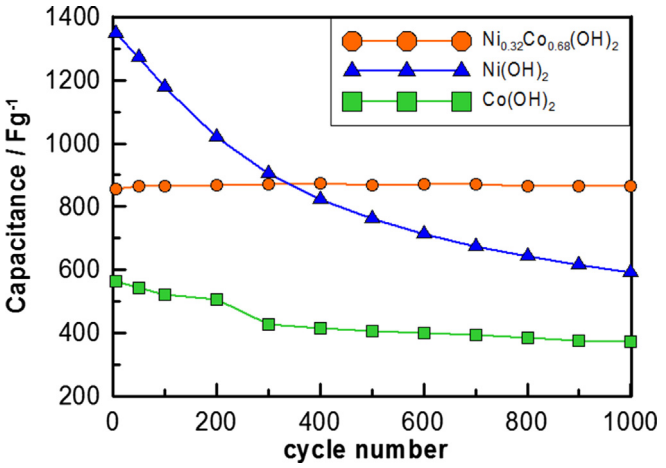

Fig. 7. The 1000-cycle stability test for $Ni(OH)_2$, $Ni_{0.32}Co_{0.68}(OH)_2$, and $Co(OH)_2$ in 1 M NaOH at 25 mV s^{-1} from −0.2 to 0.5 V.

3.6. Capacitive performances of the asymmetric design

To illustrate the excellent applicability of $Ni_{0.32}Co_{0.68}(OH)_2$ to the positive electrode materials of an asymmetric supercapacitor, the charge–discharge curves of an asymmetric supercapacitor with a negative electrode of reduced graphene oxide (denoted as GS in this work) and a positive electrode of $Ni_{0.32}Co_{0.68}(OH)_2$, $Ni(OH)_2$, and $Co(OH)_2$ are shown in Fig. 8a. Note that the upper limit of the cell voltage is set at 1.6 V although an aqueous electrolyte is employed. This result clearly demonstrates the concept of enlarging the cell voltage of an asymmetric supercapacitor employing two dissimilar materials with complementary working potential windows. From a comparison of all curves, the $Ni_{0.32}Co_{0.68}(OH)_2$–GS system shows a highly symmetric charge–discharge curve, resembling that of $Co(OH)_2$–GS. Its discharge capacity is slightly higher than that of $Ni(OH)_2$–GS even though the latter system uses more energy during the charge process. All the above characteristics reveal the superior capacitive performances of the asymmetric $Ni_{0.32}Co_{0.68}(OH)_2$–GS system (i.e., the highest energy density, largest columbic and energy efficiencies among the above three asymmetric supercapacitors).

Also note that energy efficiency is one of the great concerns in developing an electrode material for ECs. The great energy loss during the charge/discharge processes not only cuts down on the capacitive performances but also generates huge heat. The generated heat will cause rapid degradation of electrode materials in a sealed and limited volume of the cell. Fig. 8b shows the high energy efficiency of $Ni_{0.32}Co_{0.68}(OH)_2$–GS over a wide current density range in comparing with $Co(OH)_2$–GS and $Ni(OH)_2$–GS. The energy efficiency of $Ni_{0.32}Co_{0.68}(OH)_2$–GS at low current density is extremely high due to its superior reversibility in the charge storage. The decrease in the energy efficiency for $Ni(OH)_2$–GS and $Co(OH)_2$–GS with decreasing the charge/discharge current density at current densities <5 A g^{-1} is due to the significance of the irreversible reaction in the high cell voltage region (coming from the redox transitions of $Ni(OH)_2$ and $Co(OH)_2$). The contribution of the irreversible reaction becomes more significant at a lower charge–discharge current density because a longer charge time is required, leading to more wasted charges. When the current density is equal to/above 5 A g^{-1}, the contribution of the irreversible reaction becomes negligible while the *iR* drop dominates the energy efficiency which decreases with increasing the current density.

Fig. 8c shows the Ragone plot of $Ni_{0.32}Co_{0.68}(OH)_2$–GS, $Ni(OH)_2$–GS, and $Co(OH)_2$–GS asymmetric ECs. Here the results are based on

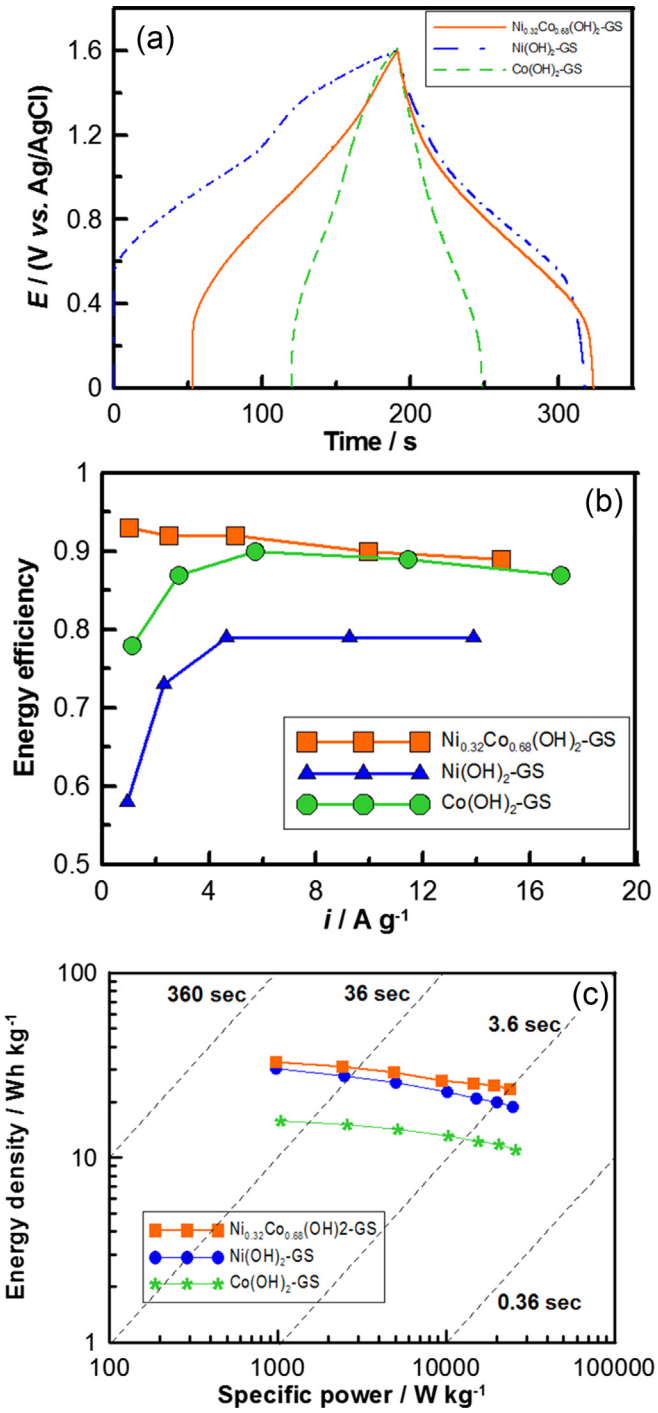

Fig. 8. (a) The charge–discharge curves measured at 4 A g^{-1} in 1 M NaOH, (b) the energy efficiency against the charge–discharge current density plot, and (c) the Ragone plot for $Co(OH)_2$–GS, $Ni(OH)_2$–GS, and $Ni_{0.32}Co_{0.68}(OH)_2$–GS asymmetric supercapacitors.

the total mass of active materials on both positive and negative electrodes. The specific energy of $Ni_{0.32}Co_{0.68}(OH)_2$–GS reaches 33 Wh kg^{-1} at a specific power of 970 W kg^{-1} meanwhile the specific power can reach 23.9 kW kg^{-1} with its specific energy equal to 24 Wh kg^{-1}. More importantly, the energy efficiency of the $Ni_{0.32}Co_{0.68}(OH)_2$–GS system is high, which avoids the joule-heating effect. All the above results and discussion reveal that $Ni_{0.32}Co_{0.68}(OH)_2$ is a promising candidate for the positive electrode materials of superior-performance asymmetric ECs with high specific energy, outstanding energy efficiency, great power capability, and good cycle stability.

4. Conclusions

Due to the involvement of electrochemical reduction of NO_3^- and chemical precipitation of hydroxides in the cathodic deposition process of hydroxides, the deposition current density, pH, temperature, and composition of the deposition bath significantly change the morphology, composition, and/or pore size of $Ni_xCo_{1-x}(OH)_2$. A porous structure consisting of vertically standing platelets is more likely formed at a small deposition current density. The pH value and deposition temperature affected the composition and morphology of $Ni_xCo_{1-x}(OH)_2$ because of the faster deposition rate of $Co(OH)_2$ in comparison with $Ni(OH)_2$. The composition of $Ni_xCo_{1-x}(OH)_2$ is almost identical to that of the deposition bath when the binary hydroxides were prepared at pH = 6 and bath temperature = 70 °C. The coincidentally negative shift in the anodic and cathodic peaks for the hydroxides with a higher Co content, the high specific capacitance, the superior rate capability, and the good cycle stability of $Ni_xCo_{1-x}(OH)_2$ can be credited to the synergistic effects of the atomic mixture of $Ni(OH)_2$ and $Co(OH)_2$. The $Ni_{0.32}Co_{0.68}(OH)_2$ deposit prepared from the bath with the Co/Ni ratio equal to 2 exhibits the high specific capacitance, and excellent capacitance rate-retention at 500 mV s^{-1}. The asymmetric supercapacitor with a positive electrode of $Ni_{0.32}Co_{0.68}(OH)_2$ and a negative electrode of reduced graphene oxide shows a superior energy efficiency in a wide range of charge–discharge current density. The specific power and energy of this asymmetric cell simultaneously reach 23.9 kW kg^{-1} and 24 Wh kg^{-1}, respectively.

Acknowledgements

The financial support from the National Science Council of ROC Taiwan under contract no. NSC-102-2221-E-007-120-MY3, 102-3113-P-006-012, 102-3113-P-194-003, and 101-2221-E-007-112-MY3, Delta-NTHU research program, and the boost program from the Low Carbon Energy Research Center of National Tsing Hua University, are gratefully acknowledged.

Appendix A. Supplementary data

Supplementary data related to this article can be found at http://dx.doi.org/10.1016/j.jpowsour.2013.12.073.

References

[1] S.A. Freunberger, Y. Chen, N.E. Drewett, L.J. Hardwick, F. Bardé, P.G. Bruce, Angew. Chem. Int. Ed. 50 (2011) 8609–8613.
[2] D.N. Prater, J.J. Rusek, Appl. Energy 74 (2003) 135–140.
[3] B.E. Conway, Electrochemical Supercapacitors, Kluwer-Plenum Pub. Co., New York, 1999.
[4] M. Winter, R.J. Brodd, Chem. Rev. 104 (2004) 4245–4270.
[5] C.C. Hu, K.H. Chang, M.C. Lin, Y.T. Wu, Nano Lett. 6 (2006) 2690–2695.
[6] J.W. Long, D. Bélanger, T. Brousse, W. Sugimoto, M.B. Sassin, O. Crosnier, MRS Bull. 36 (2011) 513–522.
[7] C.C. Hu, J.C. Chen, K.H. Chang, J. Power Sources 221 (2013) 128–133.
[8] D. Cericola, R. Kötz, Electrochim. Acta 72 (2012) 1–17.
[9] Q. Li, H. Ni, Y. Cai, X. Cai, Y. Liu, G. Chen, L.-Z. Fan, Y. Wang, Mater. Res. Bull. 48 (2013) 3518–3526.
[10] K.H. Chang, Y.T. Wu, C.C. Hu, in: V. Gupta (Ed.), Recent Advances in Supercapacitors, Transworld Research Network, India, 2006, pp. 29–56 (Chapter 3).
[11] C.C. Hu, T.-Y. Hsu, Electrochim. Acta 53 (2008) 2386–2395.
[12] T.Y. Wei, C.H. Chen, H.C. Chien, S.Y. Lu, C.C. Hu, Adv. Mater. 22 (2010) 347–351.
[13] B.B. Ezhov, O.G. Malandin, J. Electrochem. Soc. 138 (1991) 885–889.
[14] M.E. Uñates, M.E. Folquer, J.R. Vilche, A.J. Arvia, J. Electrochem. Soc. 139 (1992) 2697–2704.

[15] Y. Zhang, X. Cao, H. Yuan, W. Zhang, Z. Zhou, Int. J. Hydrogen Energy 24 (1999) 529–536.
[16] D.A. Corrigan, R.M. Bendert, J. Electrochem. Soc. 136 (1989) 723–728.
[17] Y. Ding, J. Yuan, Z. Chang, J. Power Sources 69 (1997) 47–54.
[18] M. Oshitani, H. Yufu, K. Takashima, S. Tsuji, Y. Matsumaru, J. Electrochem. Soc. 136 (1989) 1590–1593.
[19] J. Chen, D.H. Bradhurst, S.X. Dou, H.K. Liu, J. Electrochem. Soc. 146 (1999) 3606–3612.
[20] Z.A. Hu, Y.L. Xie, Y.X. Wang, H.Y. Wu, Y.Y. Yang, Z.Y. Zhang, Electrochim. Acta 54 (2009) 2737–2741.
[21] V. Gupta, S. Gupta, N. Miura, J. Power Sources 175 (2008) 680–685.
[22] J.H. Zhong, A.L. Wang, G.R. Li, J.W. Wang, Y.N. Ou, Y.X. Tong, J. Mater. Chem. 22 (2012) 5656–5665.
[23] G. Spinolo, S. Ardizzone, S. Trasatti, J. Electroanal. Chem. 423 (1997) 49–57.
[24] I. Serebrennikova, V.I. Birss, J. Electrochem. Soc. 144 (1997) 566–571.
[25] C. Lin, J.A. Ritter, B.N. Popov, J. Electrochem. Soc. 145 (1998) 4097–4103.
[26] L.C. Schumacher, I.B. Holzhueter, I.R. Hill, M.J. Dignam, Electrochim. Acta 35 (1990) 975–984.
[27] S. Trasatti, Electrochim. Acta 36 (1991) 225–241.
[28] Y.S. Lee, C.C. Hu, T.C. Wen, J. Electrochem. Soc. 143 (1996) 1218–1225.
[29] C.C. Hu, C.Y. Cheng, Electrochem. Solid-State Lett. 5 (2002) A43–A46.
[30] K. Nakaoka, M. Nakayama, K. Ogura, J. Electrochem. Soc. 149 (2002) C159–C163.
[31] I.G. Casella, M. Gatta, J. Electroanal. Chem. 534 (2002) 31–38.
[32] C.C. Hu, K.H. Chang, T.Y. Hsu, J. Electrochem. Soc. 155 (2008) F196–F200.
[33] Y. Tan, S. Srinivasan, K.S. Choi, J. Am. Chem. Soc. 127 (2005) 3596–3604.
[34] C.N.R. Rao, A.K. Sood, K.S. Subrahmanyam, A. Govindaraj, Angew. Chem. Int. Ed. 48 (2009) 7752–7777.
[35] Y.H. Lee, K.H. Chang, C.C. Hu, J. Power Sources 227 (2013) 300–308.
[36] F. Gauthard, F. Epron, J. Barbier, J. Catal. 220 (2003) 182–191.
[37] T.C. Wen, C.C. Hu, J. Electrochem. Soc. 139 (1992) 2158–2163.
[38] N. Eliaz, M. Eliyahu, J. Biomed. Mater. Res. Part A 80A (2007) 621–634.
[39] L. Su, L. Gong, J. Gao, J. Power Sources 209 (2012) 141–146.
[40] J.R.S. Brownson, C. Lévy-Clément, Electrochim. Acta 54 (2009) 6637–6644.
[41] W.H. Zhu, J.J. Ke, H.M. Yu, D.J. Zhang, J. Power Sources 56 (1995) 75–79.
[42] L.X. Yang, Y.J. Zhu, H. Tong, Z.H. Liang, L. Li, L. Zhang, J. Solid State Chem. 180 (2007) 2095–2101.
[43] L.B. Kong, J.W. Lang, M. Liu, Y.C. Luo, L. Kang, J. Power Sources 194 (2009) 1194–1201.
[44] X.M. Liu, Y.H. Zhang, X.G. Zhang, S.Y. Fu, Electrochim. Acta 49 (2004) 3137–3141.
[45] C. Nethravathi, N. Ravishankar, C. Shivakumara, M. Rajamathi, J. Power Sources 172 (2007) 970–974.